COMMUNICATION

Ion-Irradiation-Induced Defects in Isotopically-Labeled Two Layered Graphene: Enhanced In-Situ Annealing of the Damage

Martin Kalbac, Ossi Lehtinen, Arkady V. Krasheninnikov, and Juhani Keinonen*

As in conventional semiconductors, atomic scale defects[1] in graphene strongly influence its properties, and may have either detrimental or overall beneficial effects on the characteristics of the material. The examples of the former are a decrease in electron mobility[2,3] or drop in mechanical characteristics[4,5] with an increase in defect concentration. Doping through introduction of substitutional impurities[6] and adatoms, selective functionalization on defect sites,[7] and engineering the local electronic[8] as well as magnetic[9] structure through controllable creation of defects can be referred to in the context of the latter.

Numerous experiments have demonstrated that defects and impurities can efficiently be introduced in graphene by beams of energetic particles such as ions[2,3,10,11] and electrons.[12,13] Ion bombardment can be combined with post-irradiation treatment to achieve a desired functionality, e.g. by depositing metal atoms on irradiation-induced defects.[7] High dose irradiation with a focused ion beam can be used for cutting and patterning graphene with a high spatial resolution.[14–16] All these results indicate that understanding defect production in graphene under ion bombardment is mandatory for successful treatment of graphene by ion beams. At the same time, in the context of fundamental aspects of ion-solid interaction, graphene is a very unusual target. Contrary to bulk solids, every displacement of an atom from a suspended monoatomic graphene under ion irradiation should give rise to the formation of a defect, as the displaced atoms will be sputtered away, so that recombination of Frenkel pairs is not possible. Moreover, due to its truly two-dimensional structure, the probability for a collision cascade in graphene is low,[17] making the studies on defect production in graphene even more desirable.

Creation of defects in graphene under ion bombardment is also interesting in the context of quantitative assessment of the amount of irradiation-induced damage in graphene samples by Raman spectroscopy, which is an efficient tool for studying disorder and defects in sp^2-hybridized carbon materials.[16,18–21] It is known that for graphite samples the intensity ratio of the Raman D mode and the G mode is inversely proportional to the crystallite size (La).[18,20] In case of graphene one should consider point defects in the crystalline lattice rather than the crystallite size La which is more related to border defects. The concentration of defects is therefore characterized by the average distance between two point defects L_D. Lucchese et al.[22] studied the effects of Ar^+ ion irradiation on graphene made by cleaving of graphite flakes. They showed[22] that the D/G ratio is increasing with the number of defects and this ratio saturates when the distance between two defects is smaller than 3 nm. At this stage the average distance between two defects is getting shorter than the average distance traveled by an electron-hole pair before scattering with a phonon.

Here we used isotopically labeled single and bi-layer graphene sheets to study the effects of ion irradiation on such targets. The samples were formed by subsequent transfer of ^{12}C and ^{13}C graphene sheets on to a Si/SiO_2 substrate[23,24] and irradiated by Ar^+ ions with various doses. Contrary to previous studies focused on bi-layer graphene[25,26] where low energy (90 eV) ions were used, the beam energy in our experiments was 100 keV. Raman spectroscopy was used to assess the amount of damage in the samples. Our approach allowed us to distinguish the effects of ion bombardment on different graphene sheets. By combining the experimental data with the results of our molecular dynamics simulations, we show that the amount of damage after irradiation is different in the top and bottom layer, and that the difference comes from enhanced *in-situ* defect annealing (self-annealing) in the lower layer rather than from different number of defects in the layers created by the impacts of the ions.

The samples in our study were constructed by placing ^{12}C and ^{13}C graphene sheets randomly on top of each other, as schematically shown in **Figure 1**. The resulting samples have areas where the two graphene layers are stacked on one another (2-LG) with random orientation of the crystallographic axes in the graphene layers, with ^{12}C being the top-most layer, and areas where single layer ^{12}C and ^{13}C graphene (1-LG) is present. In total five samples were prepared: one for each irradiation fluence and one reference sample.

Raman spectra measured from these areas are displayed in **Figure 2**. The spectra clearly show the two main features of graphene spectra: The G and G′ modes. There is also a weak D mode, which originates from the transverse optical (TO) phonons around the K or the K′ points in the first Brillouin zone and needs defects for its activation. The D mode and its

Dr. M. Kalbac
J. Heyrovský Institute of Physical Chemistry
Academy of Sciences of the Czech Republic
v.v.i., Dolejškova 3, CZ-18223 Prague 8, Czech Republic
E-mail: martin.kalbac@jh-inst.cas.cz
Dr. O. Lehtinen, Dr. A. V. Krasheninnikov, Prof. J. Keinonen
Department of Physics
University of Helsinki
P.O. Box 43, FI-00014 Helsinki
Dr. A. V. Krasheninnikov
Department of Applied Physics
Aalto University
P.O. Box 11100, FI-00076 Aalto, Finland

DOI: 10.1002/adma.201203807

© 2013 WILEY-VCH Verlag GmbH & Co. KGaA, Weinheim

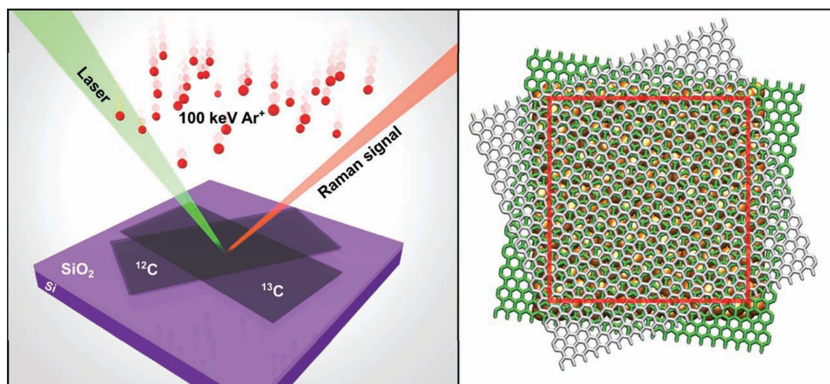

Figure 1. Schematic illustration of the experimental (left panel) and simulation (right panel) setups. The samples were formed by subsequent transfer of ^{12}C and ^{13}C graphene sheets on Si/SiO_2 substrate and irradiated by Ar^+ ions with various doses followed by Raman probing. In simulations, the area outside the red rectangle is the part of the system connected to a simulated heat bath. The ions hit the central area of the structure in a direction perpendicular to the substrate.

intensity are related to the amount of defects in graphene. The small intensity of the D mode indicates that the as-prepared samples contain negligible amount of defects.

An important feature in these spectra is the separation of the Raman bands originating from the ^{12}C and ^{13}C layers. This is a consequence of the different masses of the carbon isotopes: $(\omega_0-\omega)/\omega_0 = 1- [(12 + c_0)/(12+c)]^{1/2}$, where ω_0 is the frequency of a particular Raman mode in the ^{12}C sample, c = 0.99 is the concentration of ^{13}C in the enriched sample, and c_0 = 0.0107 is the natural abundance of ^{13}C. According to this equation, the downshift of the D, G and G′ bands for ^{13}C graphene with regard to ^{12}C graphene is expected to be 48 cm^{-1}, 56 cm^{-1} and 95 cm^{-1}, respectively, which is in a quite good agreement with our experimental results (49 cm^{-1}, 60 cm^{-1} and 98 cm^{-1}). The line width of the Raman peaks are not expected to change with a change of isotope content.

Since the orientation of the graphene layers with respect to each other is random, the Raman spectrum of the 2-LG is expected to be a combination of ^{12}C and ^{13}C Raman spectra. This is roughly the case, as evident from Figure 2. Nevertheless, a more detailed comparison of the Raman spectra of 2-LG and 1-LG spectra points to several differences, which originate from different environments of the bottom and the top layers. While the bottom layer is in contact with the substrate, the top layer interacts with atmospheric gases. Hence, the bottom layer and the top layer exhibit different levels of doping and stress. This is demonstrated for example by the smaller G′ mode of the bottom layer than observed for the top layer and also different frequencies of the G mode in 1-LG and 2-LG.

We note that the Raman features are dependent on twist angle between two layers of graphene in 2-LG. These changes are the most significant for the G mode intensity which dramatically increases for specific twist angles between graphene layers.[27] Hence, the G mode intensity is actually sensitive probe for the relative orientation of the graphene layers in 2-LG. In this study we focused on areas of the sample which did not exhibit the G mode enhancement. Other effects like a change of the FWHM or frequency are much less pronounced, hence they are not significantly affecting our measurements in this case.

In order to investigate the dependence of the Raman spectra on the density of lattice defects, the samples were exposed to 100 keV Ar^+ ion irradiation. Four samples were irradiated with total irradiation fluences of 0.12 × 10^{13} ions.cm^{-2}, 0.3 × 10^{13} ions/cm^2, 0.6 × 10^{13} ions.cm^{-2}, and 1.2 × 10^{13} ions.cm^{-2} which corresponds to approximately 1.2, 3, 6 and 12 impacts per 100 nm^2, respectively.

Raman spectra measured from ^{12}C and ^{13}C areas, as well as the 2-LG area of the sample exposed to the irradiation fluence of 0.3 × 10^{13} ions.cm^{-2}, are shown in **Figure 3**. The Ar^+ ion bombardment created defects which are manifested in the Raman spectra by increased intensity of the D peak and appearance of a new band at about 1610 cm^{-1}. This band is assigned to the D′ mode. The D′ band originates from TO phonons, but in contrast to the D mode, it involves an intravalley process connecting K and K′ points of the same Dirac cone around the K or the K′ point.[28,29]

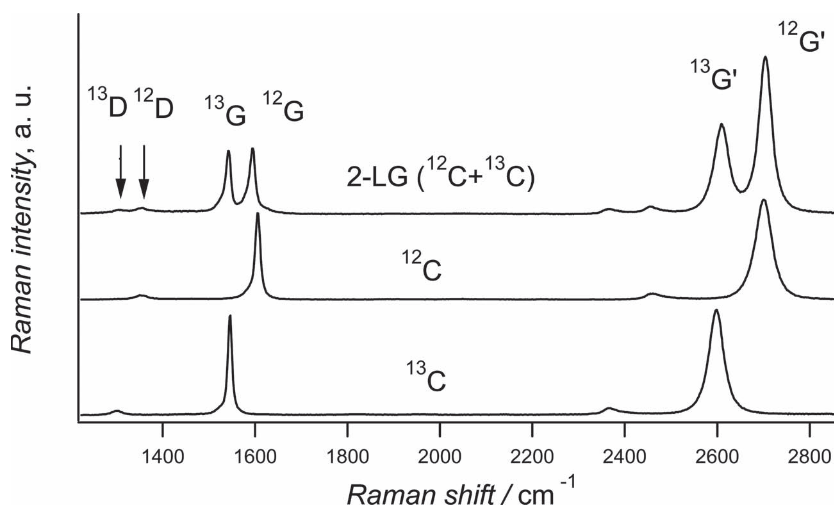

Figure 2. Raman spectra of as-prepared 1-LG ^{13}C, 1-LG ^{12}C and 2-LG (^{13}C + ^{12}C) samples. The two arrows indicate the locations of the D modes.

The Raman spectra of ^{12}C and ^{13}C 1-LG after Ar^+ ion bombardment have similar shapes. At the same time, the Raman spectrum of 2-LG graphene is obviously not simply a superposition of the irradiated 1-LG spectra. Focusing on the D/G band intensity ratio, one may easily see that it is smaller for the ^{13}C bottom layer in 2-LG than for ^{13}C 1-LG. On the other hand, the D/G ratio is similar for the ^{12}C top layer in 2-LG and ^{12}C 1-LG. The top layer in 2-LG is in contact with another graphene layer while the 1-LG is in contact with SiO_2 substrate. Therefore it appears that the differences between the

© 2013 WILEY-VCH Verlag GmbH & Co. KGaA, Weinheim

COMMUNICATION

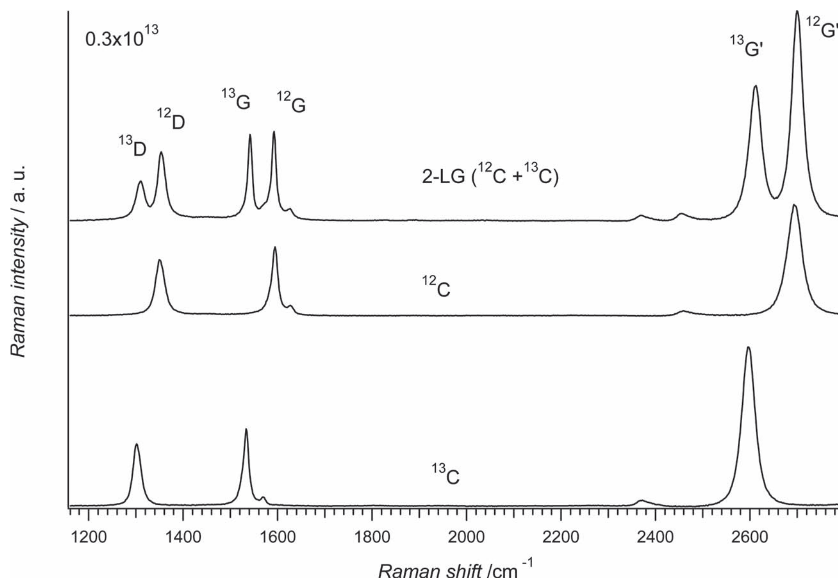

Figure 3. Raman spectra of 1-LG ^{13}C, 1-LG ^{12}C and 2-LG (^{13}C + ^{12}C) samples with intentionally created defects using Ar^+ ion bombardment. The total fluence of Ar^+ ions was 0.3 × 10^{13} ions.cm^{-2}.

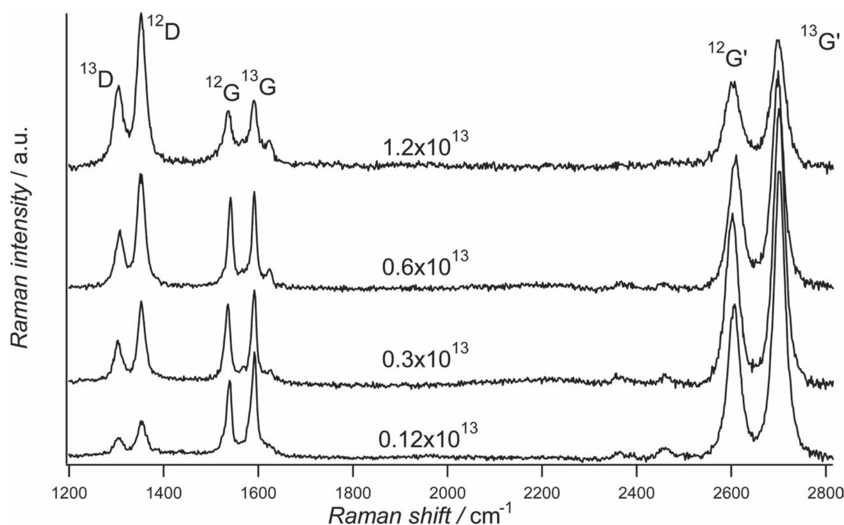

Figure 4. Raman spectra of the 2-LG graphene samples irradiated by Ar^+ ions with different fluences.

Raman spectra of 1-LG and 2-LG are not determined by the presence of the substrate.

Figure 4 shows the Raman spectra of the 2-LG graphene samples irradiated by 100keV Ar^+ ions with different fluences. The intensity of the D band increases with increasing ion fluence, while the 2450 cm^{-1} Raman mode (G*) gradually diminishes to the point of disappearance at the highest dose. In addition, at the highest fluence used (1.2 × 10^{13} ions.cm^{-2}), the intensities of the Raman bands of the main graphene features (G and G′modes) are decreased and they are significantly broadened due to phonon scattering from defects. On the other hand, we do not see any changes with increasing fluence in the Raman frequency of the G mode or the G′ mode,[30] which is in agreement with previously reported results.[24]

In order to quantify the amount of produced defects, the evolution of the D/G and D/G′ ratios were studied with increasing irradiation fluence (**Figure 5**, panels a and b). The spectra of 2-LG in Figure 4 were fitted using Lorentzian line shapes, and peak areas were calculated from these fits. We plotted the ratio of peak areas, since the peak area represents the probability of the whole Raman process, while the intensity (peak height) can be influenced by the width of the band.

The first observation here is that the changes in the Raman spectra with increasing ion fluence are bigger for the top layer than for the bottom layer graphene independent of the indicator used (D/G or D/G′ ratio). This experimental observation confirms that the effect of Ar^+ ion bombardment on the top layer is stronger than on the bottom layer of two layered graphene, and in addition it is proportional to ion fluence.

The D/G ratio does not depend linearly on irradiation dose, whereas the D/G′ ratio does. It has been shown previously that a high amount of defects can lead to a decrease of the intensity of the Raman modes.[31] Since the G´ and the D modes are activated by the

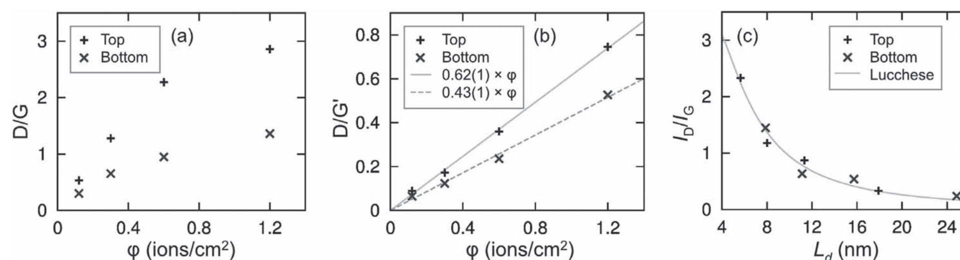

Figure 5. D/G (a) and D/G′ (b) intensity ratios as functions of Ar^+ ion irradiation fluence (in 10^{13} ions/cm^2). c) The D/G peak height ratio as fitted to the model by Lucchese et al.[22]

© 2013 WILEY-VCH Verlag GmbH & Co. KGaA, Weinheim

same phonons, the effects of defects on these modes might be similar, and therefore it should be compensated in the D/G′ ratio.

From the slopes of the linear fits to the D/G′ ratios it can be deduced that 30(2) percent fewer defects are seen in the bottom layer, as compared to the top layer. The slopes, however, do not allow quantitative estimates of the absolute number of defects produced in the sample by irradiation.

In order to estimate these values, the phenomenological model developed by Lucchese et al.[22] can be employed. In accordance with the model, the D/G intensity ratios (based on peak heights) can be fitted to an analytical function ($I_D/I_G = f\,L_D$, the form of the function is given in Ref.[22]) based on estimating the fractional sample area in which the D mode is activated, depending on the concentration of defects.

When fitting the data, it was assumed that the defect concentration increases linearly with increasing ion fluence. The defect creation probability per ion impact in each of the layers was taken as a fitting parameter. In other words, separately for each layer, a least squares fit of the relation $I_D/I_G = f\left(1/\sqrt{P \times \varphi}\right)$ was conducted, where P is the defect creation probability in the layer in question. The fitted values were 0.25(4) defects per ion in the top layer and 0.13(4) defects per ion in the bottom layer, which in turn indicate 48% fewer defects present in the bottom layer, as compared to the top layer. The experimental I_D/I_G ratios are plotted in Figure 5(c) with the L_D values calculated using the fitted values of P along with Lucchese's function for reference.

These results raise a question: Why are there fewer defects in the bottom layer? The projected range of 100 keV Ar^+ ions in graphite is approximately 80 nm,[32] meaning that the ions easily penetrate the two graphene layers. In the binary collision model routinely employed for estimating ion irradiation damage[32] the defect concentration mainly depends on the rate of energy loss of the ion, which in turn depends on the total energy of the ion. Within this model, there should be no significant difference between damage in the top and bottom graphene layers. Collision cascades do contribute to the total damage, but the cascades progress rather in the direction of the ion trajectory than towards the surface, meaning the damage rate should be higher in the bottom layer, if cascades had an important effect.

It is also unlikely that the substrate is responsible for different effects of Ar^+ ions on the top and bottom layer. If the substrate would make a difference, for example due to trapped charges created by Ar^+ ions in the substrate, one would expect a stronger effect on the bottom layer than on the top layer. In addition, we can exclude the influence of trapped charges created in SiO_2 substrate by ion bombardment, since there is no signature of any changes in graphene doping level in the Raman spectra: Doping would cause a change in the Raman frequency, which is not observed experimentally here. Also, the measurements from the 1-LG areas in the sample show that the proximity of the substrate to the graphene layers does not reduce the amount of produced damage.

In order to attain microscopic insight into the physical processes taking place during ion irradiation, we turned to analytical potential molecular dynamics simulations. The effects of energetic ion impacts on the sample were modeled, and estimates of the number of defects created and the number of atoms sputtered away from each of the layers were extracted. The simulations confirmed what was assumed based on the binary collision model: Roughly equal numbers of defects are produced in both of the layers at the rate of 0.2 defects/impact, which agrees with the experimental value for the top layer, but not the bottom one.

Based on the analysis of the MD data, it can be concluded that further changes are introduced in the samples after the ion irradiation, which leads to a marked difference in the final defect densities in the graphene layers: Either additional damage is produced in the top layer, or the rate of in-situ healing of defects in the bottom layer is higher. We stress that considerable *in-situ* (self-annealing) in graphite and bi-layer graphene should be possible, as small migration barriers (less than 1 eV) for interstitial-type defects in graphene[30] makes them mobile even at room temperature.

The samples were exposed to air in between the irradiation treatments and Raman measurements. It is well known that defect sites are much more reactive than pristine graphene, and the top layer in our samples is more exposed to possibly reactive molecules. On the other hand, one would expect chemical reactions to rather increase the size of the defects than the number of defects, and the average distance between defects (which is probed by Raman spectroscopy) is mostly governed by the number of defects.

As carbon atoms are sputtered away from the graphene sheets by ion impacts, a source of extra carbon is needed to be available in order to heal the produced defects. The simulations reveal that such a reservoir does exist in the samples after ion irradiation. Many of the displaced atoms are stuck in between the two graphene layers, or in between the bottom layer and the substrate (**Figure 6**) as interstitials.

According to our MD simulations, interstitials are produced at the rate of 0.160(8) per ion in between the graphene layers and 0.35(2) in between the bottom layer and the substrate. The interstitial C atoms in between the graphene layers are available for annihilation with vacancies in both of the layers, whereas the atoms stuck in between the bottom layer and the substrate are available only to the bottom layer. In the simulations, atoms are sputtered at rates of 0.49(2) and 0.68(3) per impact from the top and bottom layers, respectively. If these values are reduced according to the number of interstitials available to each layer, the numbers change to 0.41(2) lost atoms/impact from the top layer and 0.25(3) lost atoms/impact from the bottom layer, indicating 39(8)% fewer missing atoms from the bottom layer, which is well in line with the experimental results. Here we assume the extreme case that each of the interstitials annihilate with a vacancy. If a smaller portion of the interstitials annihilate, the reductions in the sputtering rates should be scaled down accordingly.

We would like to stress here that although the C interstitial in its lowest energy configuration (the "spiro-interstitial") should not be mobile at room temperature,[33] this configuration is separated by a relatively high energy barrier from other configurations, both likely appearing after ion impacts, so that a considerable number of interstitials should be available for recombination with vacancies. Further on, the "spiro-interstitial" configuration is not necessarily possible between our

© 2013 WILEY-VCH Verlag GmbH & Co. KGaA, Weinheim

COMMUNICATION

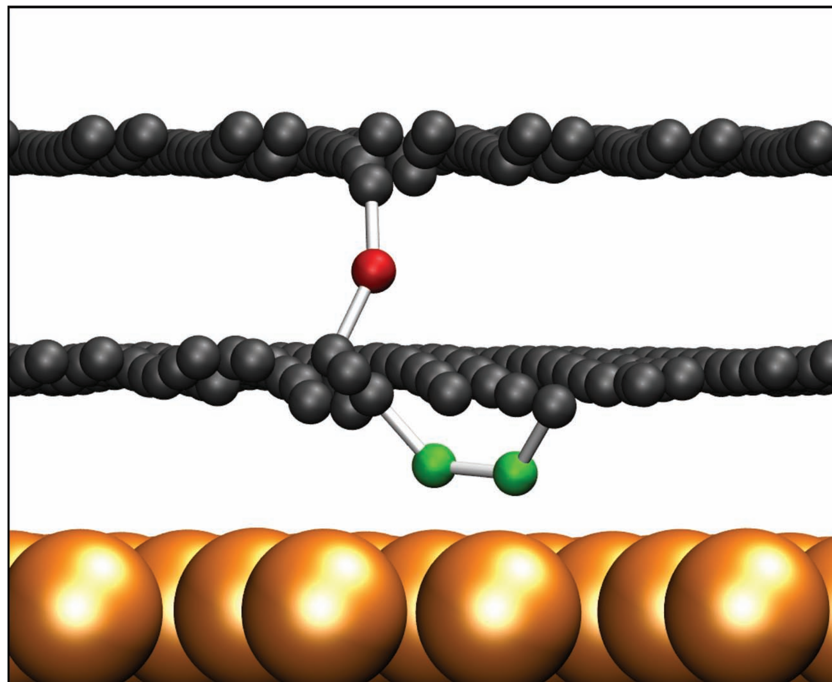

Figure 6. Snapshot from molecular dynamics simulations showing a typical atomic configuration after an ion impact. A carbon atom stuck in between the graphene layers (red sphere) and in between the bottom layer and the substrate (green spheres) are visible. Small spheres represent C atoms, big ones Si substrate atoms.

randomly oriented graphene layers and certainly not in between the bottom graphene layer and the substrate.

We would further like to point out that there may be a weak effect related to different diffusivities of carbon interstitials located in between the graphene layers and in between the bottom layer and the substrate, so that carrying out the experiments at different temperatures may give rise to different ratios between the interstials in the two regions shown in Figure 6. Thus even interstitial diffusivity measurements can be carried out with such a setup.

To conclude, by combining ion-irradiation experiments followed by the characterization of the samples using Raman spectroscopy together with atomistic simulations, we have studied the effects of 100 keV Ar^+ ion irradiation on isotopically labeled single and two-layer graphene samples for various unspecified twist angles. Based on the defect-related changes in the D/G and D/G′ band intensity ratios, it is evident that the number of defects in both of the graphene layers increases with increasing irradiation fluence, as expected, but the rate of defect accumulation significantly differs in the layers with the final defect density in the bottom layer being lower than in the top layer. The latter observation is contrary to what can be expected based on the binary collision model (a method routinely used for assessing ion irradiation damage) and analytical potential molecular dynamics simulations, which predict the same number of defects to be produced in both of the layers. This discrepancy was explained via a detailed analysis of the final locations of interstitial carbon atoms produced by sputtering by the energetic ion in the atomistic simulations. A significantly higher number of interstitials was produced in between the bottom layer and the substrate. As these interstitials are expected to be mobile at room temperature, they can recombine with vacancies in the bottom layer resulting in the reduction of total damage. Our results indicate that self- annealing of defects in two-dimensional materials may be particularly important and should be taken into account when irradiation by energetic ions is used[25] to tailor the properties of graphene and other 2D systems.

Experimental Section

Graphene samples were synthesized using the CVD method according procedure reported previously.[34] In brief: A Cu foil was heated to 1000 °C and annealed for 20 min under flowing H_2 gas. Then the film was exposed to H_2 and CH_4 for 15 minutes and finally the substrate was cooled down from 1000 °C to 500 °C under flowing H_2 and CH_4 gas. For the preparation of ^{13}C graphene, $^{13}CH_4$ was used as a feedstock (^{13}C content 99%, Aldrich). The as-grown graphene was subsequently transferred to a clean SiO_2/Si substrate using polymethylmethacrylate (PMMA), according to procedures reported previously.[35] In order to obtain 2-LG, the second layer was transferred onto 1-LG using the same procedure for the second time, thus obtaining two layers with no interlayer stacking orientation. The 2 layers of CVD graphene are expected to have random respective orientations of the layers. In some specific cases of orientation, the interaction of the layers may lead to enhancement of the Raman signal of the G-mode.[27] In our study here we focused on areas which did not exhibit the enhancement hence the latter effect should not influence our conclusions.

The samples were irradiated employing a 500 kV ion implanter unit. The used ions were 100 keV Ar^+ ions, and the initially produced focused ion beam was fed through a rasterizing unit ensuring a homogenous particle fluence on the entire sample. The irradiation fluence was determined using four Faraday cups placed inside the irradiation area.

The Raman spectra were excited by 2.41 eV laser excitation energy using a mixed Ar^+/Kr^+ laser (Coherent) and measured using micro-Raman setup LabramHR (Horiba Jobin-Yvon).

Molecular Dynamics Simulations: Analytical potential molecular dynamics simulations were conducted using the PARCAS code[33] The same method has been used earlier for simulating the interactions of energetic ions and graphene.[16,17] The simulated structure consisted of two randomly oriented and periodically translated 1196 atom graphene layers (with the atomic mass in the lower layer adjusted to 13 amu) with a 3.35 Å spacing. The actual value of the interlayer separation between the sheets in the bilayer graphene may be affected by local stacking order. Besides, it may also will also change locally due to additional van der Waals interaction of the top layer with the substrate ("through" the bottom layer), as advanced DFT calculations indicate.[36] All these effects are beyond our simple theoretical model. However, as DFT simulations also indicate that interstiatial formation energies do not differ much in bulk graphene and bilayer graphene,[33] we expect that the model should provide at least qualitative insight into the behavior of the system. The stacked layers were placed on top of a Si [111] slab of 30 Å thickness with a 3.7 Å spacing (the oxide layer was excluded from the model). The relatively thin substrate does not necessarily model all backscattered particles originating from deeper in the sample, but rather models the role of the substrate on inhibiting the motion of sputtered C atoms. The C-C interactions were described using the Brenner second

© 2013 WILEY-VCH Verlag GmbH & Co. KGaA, Weinheim

generation analytical reactive bond-order potential,[37] the C-Si and Si-Si interactions using the Erhart Si-C potential.[38] The Ar-C and Ar-Si interaction was modeled using the Ziegler-Biersack-Littmark universal repulsive potential.[32] The system was connected to a heat bath using the Berendsen thermostat at the edges outside the impact area in order to allow heat introduced by the impinging ion to be dissipated.

Acknowledgements

This work was supported by the Czech Grant agency (P208/12/1062). We further acknowledge support by the Finnish Cultural Foundation, the Academy of Finland through projects 130852, 218545, and 263416, as well as generous grants of computer time provided by CSC Finland.

Received: September 12, 2012
Published online: November 26, 2012

[1] F. Banhart, J. Kotakoski, A. V. Krasheninnikov, *ACS Nano* **2011**, *5*, 26.
[2] G. Buchowicz, P. R. Stone, J. T. Robinson, C. D. Cress, J. W. Beeman, O. D. Dubon, *Appl. Phys. Lett.* **2011**, *98*, 032102.
[3] J. H. Chen, W. G. Cullen, C. Jang, M. S. Fuhrer, E. D. Williams, *Phys. Rev. Lett.* **2009**, *102*, 236805.
[4] X. Zhang, K. Jiao, P. Sharma, B. I. Yakobson, *J. Mech. Phys. Solids* **2006**, *54*, 2304.
[5] J. R. Xiao, J. Staniszewski, J. W. Gillespie, *Comp. Struct.* **2009**, *88*, 602.
[6] O. L. Krivanek, M. F. Chisholm, V. Nicolosi, T. J. Pennycook, G. J. Corbin, N. Dellby, M. F. Murfitt, C. S. Own, Z. S. Szilagyi, M. P. Oxley, S. T. Pantelides, S. J. Pennycook, *Nature* **2010**, *464*, 571.
[7] H. T. Wang, Q. X. Wang, Y. C. Cheng, K. Li, Y. B. Yao, Q. Zhang, C. Z. Dong, P. Wang, U. Schwingenschlogl, W. Yang, X. X. Zhang, *Nano Lett.* **2012**, *12*, 141.
[8] L. Tapaszto, G. Dobrik, Nemes-Inc, G. Vertesy, P. Lambin, L. P. Biro, *Phys. Rev. B* **2008**, *78*, 233407.
[9] R. Nair, M. Sepioni, I. L. Tsai, O. Lehtinen, J. Keinonen, A. V. Krasheninnikov, C. Thomsen, A. Geim, I. V. Grigorieva, *Nat. Phys.* **2012**, *8*, 199.
[10] G. Compagnini, F. Giannazzo, S. Sonde, V. Raineri, E. Rimini, *Carbon* **2009**, *47*, 3201.
[11] B. D. Guo, Q. A. Liu, E. D. Chen, H. W. Zhu, L. A. Fang, J. R. Gong, *Nano Lett.* **2010**, *10*, 4975.
[12] J. Kotakoski, A. V. Krasheninnikov, U. Kaiser, J. C. Meyer, *Phys. Rev. Lett.* **2011**, *106*, 105505.
[13] D. Teweldebrhan, A. A. Balandin, *Appl. Phys. Lett.* **2009**, *94*, 013101.
[14] M. C. Lemme, D. C. Bell, J. R. Williams, L. A. Stern, B. W. H. Baugher, P. Jarillo-Herrero, C. M. Marcus, *ACS Nano* **2009**, *3*, 2674.
[15] D. C. Bell, M. C. Lemme, L. A. Stern, J. R. Williams, C. M. Marcus, *Nanotechnology* **2009**, *20*, 455301.
[16] O. Lehtinen, J. Kotakoski, A. V. Krasheninnikov, J. Keinonen, *Nanotechnology* **2011**, *22*, 175306.
[17] O. Lehtinen, J. Kotakoski, A. V. Krasheninnikov, A. Tolvanen, K. Nordlund, J. Keinonen, *Phys. Rev. B* **2010**, *81*, 153401.
[18] F. Tuinstra, J. L. Koenig, *J. Chem. Phys.* **1970**, *53*, 1126.
[19] C. Thomsen, S. Reich, *Phys. Rev. Lett.* **2000**, *85*, 5214.
[20] A. C. Ferrari, J. Robertson, *Phys. Rev. B* **2000**, *61*, 14095.
[21] R. Saito, A. Jorio, A. G. Souza, G. Dresselhaus, M. S. Dresselhaus, M. A. Pimenta, *Phys. Rev. Lett.* **2002**, *88*, 027401.
[22] M. M. Lucchese, F. Stavale, E. H. M. Ferreira, C. Vilani, M. V. O. Moutinho, R. B. Capaz, C. A. Achete, A. Jorio, *Carbon* **2010**, *48*, 1592.
[23] M. Kalbac, H. Farhat, J. Kong, P. Janda, L. Kavan, M. S. Dresselhaus, *Nano Lett.* **2011**, *11*, 1957.
[24] M. Kalbac, J. Kong, M. S. Dresselhaus, *J. Phys. Chem. C* **2012**, *116*, 19046.
[25] E. H. M. Ferreira, M. V. O. Moutinho, F. Stavale, M. M. Lucchese, R. B. Capaz, C. A. Achete, A. Jorio, *Phys. Rev. B* **2010**, *82*, 125429.
[26] A. Jorio, M. M. Lucchese, F. Stavale, E. H. M. Ferreira, M. V. O. Moutinho, R. B. Capaz, C. A. Achete, *J. Phys.-Condens. Matter* **2010**, *22*, 334204.
[27] M. Kalbac, O. Frank, J. Kong, J. Sanchez-Yamagishi, K. Watanabe, T. Taniguchi, P. Jarillo-Herrero, M. S. Dresselhaus, *J. Phys. Chem. Lett.* **2012**, *3*, 796.
[28] S. Piscanec, M. Lazzeri, F. Mauri, A. C. Ferrari, J. Robertson, *Phys. Rev. Lett.* **2004**, *93*, 185503.
[29] S. Piscanec, M. Lazzeri, J. Robertson, A. C. Ferrari, F. Mauri, *Phys. Rev. B* **2007**, *75*, 035427.
[30] M. Kalbac, A. Reina-Cecco, H. Farhat, J. Kong, L. Kavan, M. S. Dresselhaus, *ACS Nano* **2010**, *4*, 6055.
[31] L. G. Cancado, A. Jorio, E. H. M. Ferreira, F. Stavale, C. A. Achete, R. B. Capaz, M. V. O. Moutinho, A. Lombardo, T. S. Kulmala, A. C. Ferrari, *Nano Letters* **2011**, *11*, 3190.
[32] J. F. Ziegler, M. D. Ziegler, J. Biersack, *The stopping and range of ions in matter*; SRIM, SRIM Co., Chester, Marylend **2008**.
[33] A. Gulans, A. V. Krasheninnikov, M. J. Puska, R. M. Nieminen, *Phys. Rev.B* **2011**, *84*, 024114.
[34] X. S. Li, W. W. Cai, J. H. An, S. Kim, J. Nah, D. X. Yang, R. Piner, A. Velamakanni, I. Jung, E. Tutuc, S. K. Banerjee, L. Colombo, R. S. Ruoff, *Science* **2009**, *324*, 1312.
[35] A. Reina, X. T. Jia, J. Ho, D. Nezich, H. B. Son, V. Bulovic, M. S. Dresselhaus, J. Kong, *Nano Lett.* **2009**, *9*, 30.
[36] T. Bjorkman, A. Gulans, A. V. Krasheninnikov, R. M. Nieminen, *Phys. Rev. Lett.* **2012**, *108*, 235502.
[37] D. W. Brenner, O. A. Shenderova, J. A. Harrison, S. J. Stuart, B. Ni, S. B. Sinnott, *J. Phys.-Condens. Matter* **2002**, *14*, 783.
[38] P. Erhart, K. Albe, *Phys. Rev. B* **2005**, *71*, 035211.

© 2013 WILEY-VCH Verlag GmbH & Co. KGaA, Weinheim